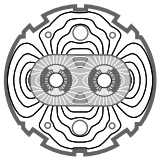

LHC Project Note 273

13 December 2001
Keith.Potter@cern.ch

Calculation of the machine induced background in IR2 of the LHC using new residual gas density distributions

I. Azhgirey*, I. Baishev*, K.M. Potter and V. Talanov*

Keywords: losses, cascade, muon

Summary

In this note we present estimations for the fluxes of the secondary particles, induced by the proton losses in IR2 of the LHC, using estimated profiles of the realistic residual gas density in the machine.

Introduction

The methodical study of the *machine induced background* — secondary particle fluxes, induced by the losses of the beam protons in the machine — was recently made for IR8 of the LHC. The estimations of the particle fluxes, resulting from the proton losses upstream and downstream of IP8, were based on published data on the residual gas composition and pressure in the different parts of the LHC. These estimations showed that the contributions from the elements of the arc cell, dispersion suppressor and straight section reflect both mechanical and magnetic structure of the machine in the region of the study. As it was also concluded, the introduction of the real gas pressure profiles can lead to significant changes in the secondary particle field formation.

There were no realistic estimations of the residual gas densities in the LHC at the moment of that study, so the previous results were given per unit of linear density of beam–gas interactions. Since then, the new calculations of the average gas densities in the vacuum chamber of the LHC interaction regions were completed citemal3. Below we study the machine induced background in the IR2, using these estimations of gas pressure and composition, available for the different scenarios of LHC operation.

Gas densities in the vacuum chamber of the IR2

The values of the residual gas densities determine the rate of the beam protons losses in a particular section of the machine and thus the absolute values of the machine induced

*Institute for High Energy Physics, Protvino, Russia.
Member of the Russian collaboration to the LHC Project.

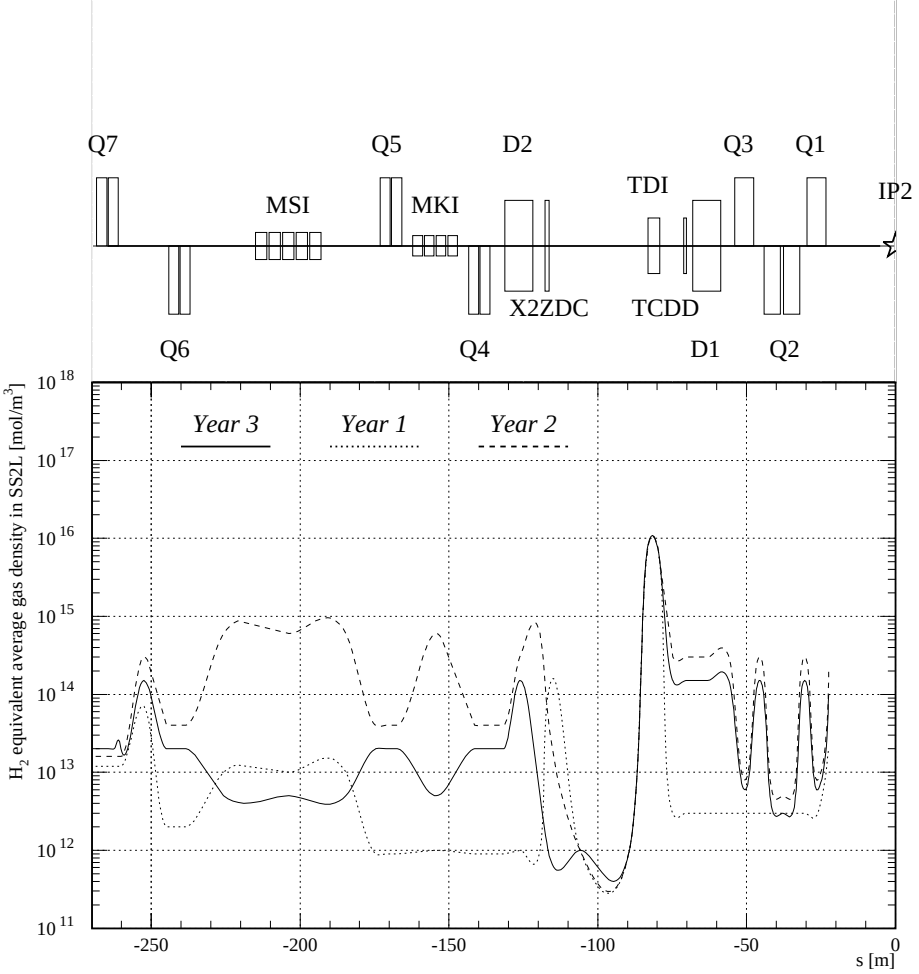

Figure 1: The profiles of H_2 equivalent average gas density in the SS2L.

background [2]. Recently numbers became available for the H_2 equivalent average gas density in the vacuum chamber of the IR2 LSS, together with the residual gas composition in the cryogenic and room temperature vacuum chambers [1]. The resulting profiles of the gas density in the SS2L of the IR2 are given in Fig. 1, for the three scenarios of the LHC operation — a basic one, "3rd year +90 days", labeled *Year 3*, and for two other cases, "1st year after 70 days" and "2nd year +10 days", labeled *Year 1* and *Year 2* respectively. At the top of the figure a sketch of the corresponding machine structure is given, which includes all the major elements of the straight section.

As can be seen from the plot, the highest values correspond to the case of the second year of LHC operation, and the lowest — in average for the first year, while the third year falls in the middle of these two. In each case the peak values are associated with the interconnections between the magnets, both cryogenic, as in the case of the inner triplet, and the room temperature ones in the matching section. All three distributions are featured by a sharp peak at the position of the TDI absorber where the value for the equivalent gas density of 10^{16} mol/m^3 is about two orders of magnitude higher than the values for the neighboring elements. In addition, the interconnection between the Q6 and Q5 quadrupoles is significant. The value for the gas density there is not so high as in the TDI region, but the appeciable length of this section of about 60 m results in the significantly high integral value for the beam–gas interactions rate along this part of the structure.

As for the dispersion suppressor and arc cells, the common value of the gas density is given for these part of the LHC. It equals 4×10^{12} mol/m^3 for the third year case, 10^{13} mol/m^3 for the first year after 70 days of LHC operation, and 3×10^{13} mol/m^3 after 10 days of the second year. The given numbers can be compared with the previously published data on the residual gas composition [3], taking into account the already estimated values for the machine background, induced by the proton losses in the arc cell, dispersion suppressor and straight section of IR8 [4]. This allows one to conclude that the limitation of the studied region only to the straight section part of IR2 will be sufficient to estimate the values of secondary fluxes, induced by the beam–gas interaction, with an acceptable accuracy.

Particle cascades simulation

The calculated profiles of the residual gas densities in the vacuum chamber of the SS2 were folded with the results of the machine induced background simulation, which was done according to the methodical approach, presented in [4]. The layout of the left straight section part of the IR2, used in the simulations, is given in Fig. 2. Most of it resembles the layout of the right straight section part in the IR8, which also houses the injection line, with slightly different distances between the machine elements. The main changes are concentrated in the region between the separation dipoles D2 and D1, where a conical transition, instead of the twin aperture vacuum chamber, starts after the X2ZDC up to the TDI absorber. These elements, together with the additional shielding TCDD, protecting the D1 dipole, were introduced in the geometry, according to the current design [5]. The parameters of the magnets in the SS2 were taken from the LHC lattice version 6.3 and supplemented by the geometrical apertures of the magnetic elements and drifts [6], using the same mechanical models of the LHC magnets, as in the study for IR8.

Interactions of the beam protons with the nucleus of the residual gas in SS2 and the transport of the secondary cascades were simulated by the IHEP MARS program [7]. The overall threshold of 20 MeV on the particle kinetic energy was applied to the simulation of the transport for both hadrons and muons. Secondary particles were transported along SS2 up to the scoring plane, where the trajectory of each particle was cut and particle characteristics were recorded. The scoring plane was positioned at 1 m from the front surface of the Q1 quadrupole, that gave the distance of about 22 m between the scoring plane and the IP2, leaving the first two compensating dipoles MCBW and MBXW outside the region of the

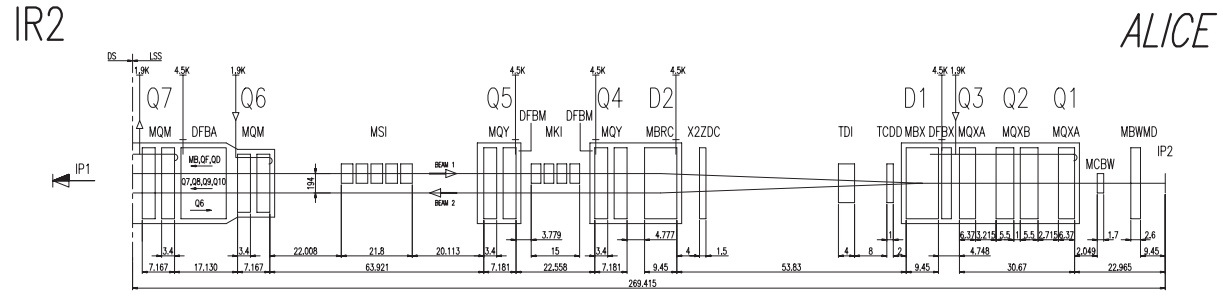

Figure 2: The layout of the SS2L. Optics version 6.3.

study.

The recorded characteristics of the secondary particles included particle kinetic energy, direction cosines and coordinates of particle track crossing the scoring plane. To provide the subsequent reconstruction of secondary particle fields in the presence of the residual gas density distribution, each particle track was tagged with the distance to the IP2 from the point of the primary proton–nucleus collision, and the type of the residual gas nucleus, with which the interaction occurred. In addition, for each particle which fell into the recorded source, the coordinates of the hadron–nucleus interaction point were kept, where this particular hadron was born, or, for muons, the parent pion. This made it possible to trace back the history of the background particles and not only to study the contribution to the machine induced background from different parts of the IR2, but also to spot the sections where most of the secondary particles that reach the experimental zone escape from the structure of the machine.

Secondary particle fluxes around IP2

The results of the simulations, folded with the gas density profiles in the IR2, are presented in Figures 3–6. The first two figures give the number of hadrons and muons, entering the UX25 cavern from the IP1 side, as a function of the primary proton–nucleus interaction distance to the IP2. As can be seen, the $n(S)$ distributions in these figures follow the shape of the corresponding profiles of the gas density from Fig. 1. This fact agrees with the results of the machine induced background formation study in the IR8, which showed that the relative contribution to the secondary fluxes around the interaction point from the beam–gas interactions is constant for most parts of the straight section [4]. The differencies, observed previously in the relative distributions in the D2–D1 and Q3–Q1 regions, are practically masked by the much sharper changes in the gas density.

The values of secondary muon flux in the region, close to the entrance of the UX25 cavern, can be obtained by integrating the given distributions along the S axis. This gives the value of 1.03×10^6 muons/s for the muon flux under the "3rd year +90 days" LHC running conditions, and the values of 0.17×10^6 and 0.75×10^6 muons/s, for the "1st year after 70 days" and "2nd year +10 days" cases, respectively. The relatively smaller values for the first two years of the accelerator run reflect the decreased value of the nominal current at that period, which is assumed to be 20 % in the first year, and 30 % in the second year of LHC operation. As for the values of the secondary hadron flux, they are about an order of magnitude higher than the corresponding muon flux values for all three cases.

In the basic case, after 90 days of LHC operation in the third year, about 80 % of the background appears to be induced by the beam–gas interactions in the region of the TDI absorber. Among the other auxillary peaks in the gas density profiles, the most significant increases can be seen in the MSI and MKI region for the case of the second year opeation, but even there it does not exceed the effect of the peak in the TDI. Thus the region of the injection shielding is currently the most critical region of the straight section in IR2, because of the residual gas density.

The results, presented in Figures 5 and 6, show the secondary fluxes in IR2 from a different point of view. These two figures give the number of hadrons and muons, entering the UX25 cavern from the IP1 side, as a function of the distance to the IP2 from the

point of the hadron–nucleus interaction, where a particular hadron was born, or, for muons, from the origin of the parent pion. Since these distributions are obtained using the same normalization, as those in Figures 3 and 4, they present the same integral values for the secondary fluxes, but distributed in a different way along the S axis of the straight section. So by their definition Figures 5 and 6 show the sections of the machine structure, where the actual background particles, rather than their ancestors, are produced.

The distributions of hadrons in Fig. 5 demonstrate that the particles that interact with the nuclei of the residual gas, for example, around the TDI, do not necessarily produce a secondary cascade, which will contribute to the background, in the region close to the point of the primary interaction. The distributions still have distinct peaks in the position of the TDI, formed by the particles, escaping directly from the TDI–D1 drift space. But in the new representation this peak is now followed by a further increase along the inner triplet, illustrating the previously discussed "bottleneck" effect [8]. Generally for all three profiles of the gas density, the closer to the scoring plane the region of the last interaction, the more secondary hadrons are collected from it. As for the muon distributions, the length of the D2–Q1 section almost constantly contributes to the resulting background, with the peaks in between the elements, where parent pions are not stopped by the material of the magnets.

The Figures 7–10 show the influence of the gas density peak in the TDI region on the secondary fluxes in the downstream parts of the straight section. These distributions were obtained assuming the same average gas density in the TDI as in the element closest to it, which is the D1 dipole. While Figures 7 and 8 obviously differ from the previous ones only by the disappearance of the TDI peak, in Figures 9 and 10 all the curves are down in the TDI–Q1 section by nearly an order of magnitude. This reflects the decreased number of the particles from the primary interactions, that reach this region to start the secondary cascades.

The final set of Figures 11–14, produced with the same assumption on the gas density in the TDI, represents a first look at the energy distribution of the background, produced in the straight section. Secondary particles with kinetic energy below 1 GeV were excluded. Thus Figures 13 and 14 give the origin of the hard, high energy, component of the machine induced background, which is supposed to be the main hazard for the equipment in the experimental zones because of its high penetration ability. It was noted already that the scoring plane, being positioned just in front of the Q1 quadrupole, collects most of the high-angular, low-energy secondaries, produced in the region of downstream low–β Q3–Q1 triplet [4]. As can be seen, the introduction of the 1 GeV cut on the particle kinetic energy, excluding the low energy component of the background, leads to a further decrease of the secondary fluxes, produced by the cascades in the inner triplet region. Under these conditions, the D2–D1 region appears to be the primary source of the machine induced background around IP2, since the main portion of the high energy secondary muons that reach the UX25 cavern are produced there.

Conclusion

The introduction of realistic profiles for the average residual gas density in the machine induced background simulations in IR2 enables the estimation of contributions of secondary particle fluxes from the different parts of the straight section SS2. The new estimates can be

compared with the ones that were obtained for IR8 and which were based on the previously published data on the residual gas composition. This comparison shows an increase by a factor of 5 in the secondary muon and hadron flux at the entrance to the experimental cavern. At the same time the new results show that for the scenarios of the long–term LHC operation the region of the TDI absorber is the main source of the secondary cascades in the downstream part of the straight section. Further study gave the indication that under the assumption of the gas density in the TDI, decreased to the D1 level, and with the exclusion of the low energy component of the background, the D2–D1 transition becomes the region of primary importance.

Appendix

In addition to the results discussed above, Figures 16–19 give the same distributions for the two other periods of LHC operation, namely "1st year beginning" and "2nd year beginning" ones. The normalisation of calculated particle fluxes on the average gas densities for these two cases gives the value of $0.12 \div 4.11 \times 10^7$ muons/s for the machine induced muons flux at the entrance of UX25 cavern. Although representing the somehow extremal conditions of the machine operation, these values nevertheless indicate the rates of the secondary particles in IR2 at LHC starting scenarios.

References

[1] I.R. Collins *et al*, LHC Project Note (to be published).

[2] I. Azhgirey *et al*, In: One Day Workshop on LHC Backgrounds, CERN, March 22, 1996.

[3] A. Mathewson, In: One Day Workshop on LHC Backgrounds, CERN, March 22, 1996.

[4] I. Azhgirey *et al*, LHC Project Note 258, Geneva, CERN, 2001.

[5] The minutes of the Working Group on LHC Injection.
`http://lhc-injwg.web.cern.ch/lhc-injwg/InjWG_minutes.htm`

[6] J.B. Jeanneret, private communication.

[7] I. Azhgirey and V. Talanov, In: Proc. of XVIII Workshop on the charged particles accelerators, Protvino, 2000, vol. 2, p. 184–187.

[8] I. Baishev *et al*, LHC Project Report 500, Geneva, CERN, 2001.

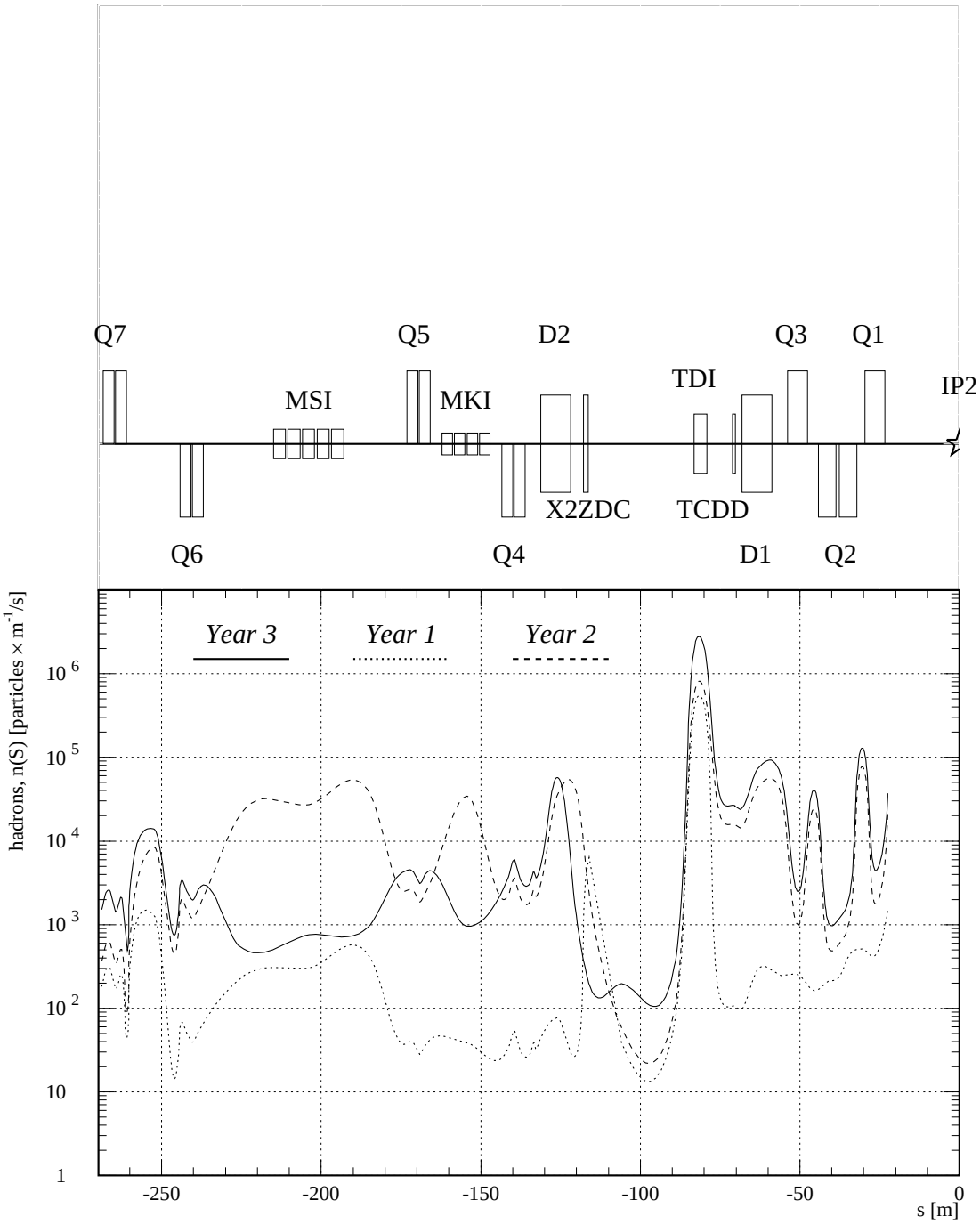

Figure 3: Number of hadrons, entering the UX25 cavern from the IP1 side, as a function of primary proton–nucleus interaction distance to the IP2.

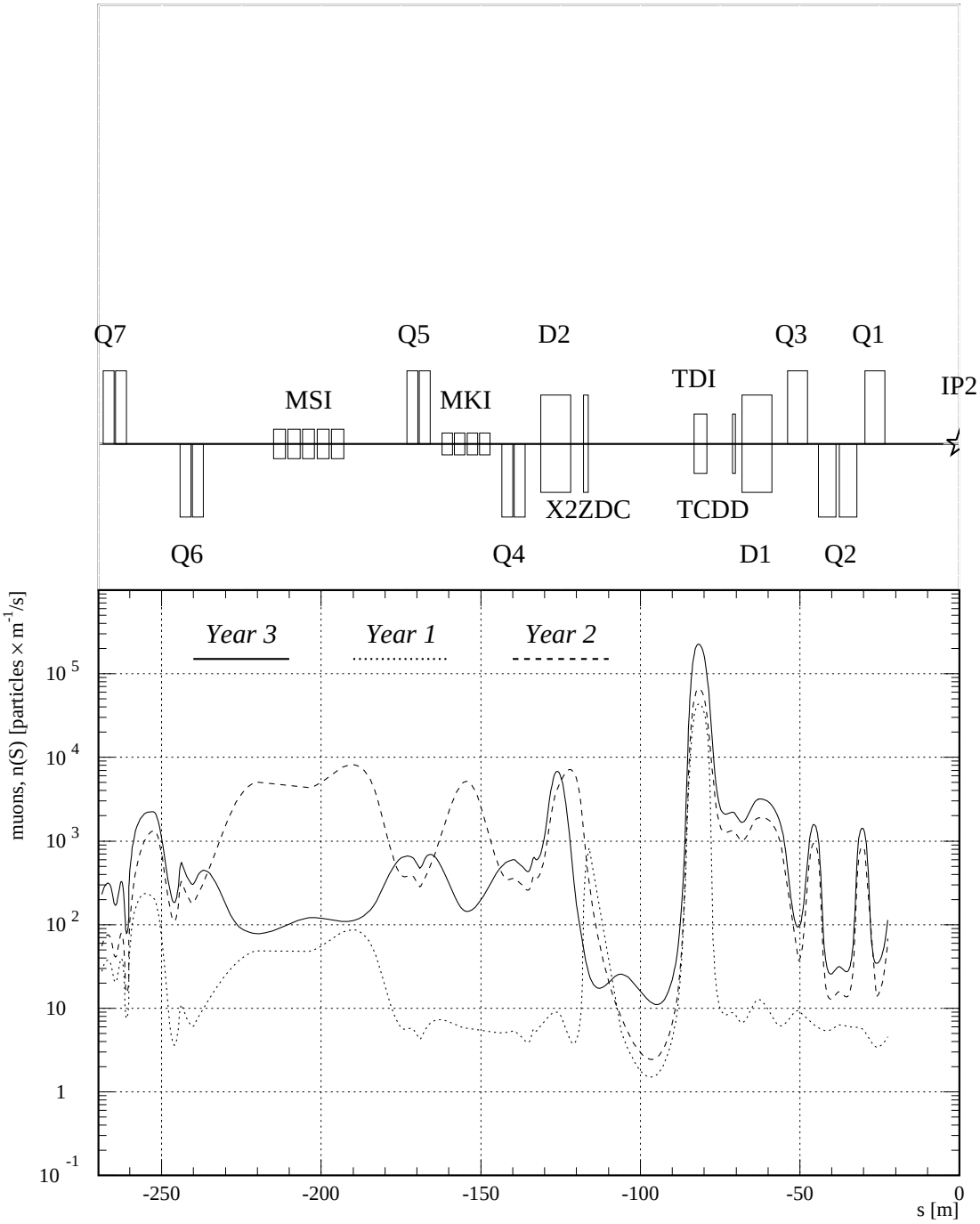

Figure 4: Number of muons, entering the UX25 cavern from the IP1 side, as a function of primary proton–nucleus interaction distance to the IP2.

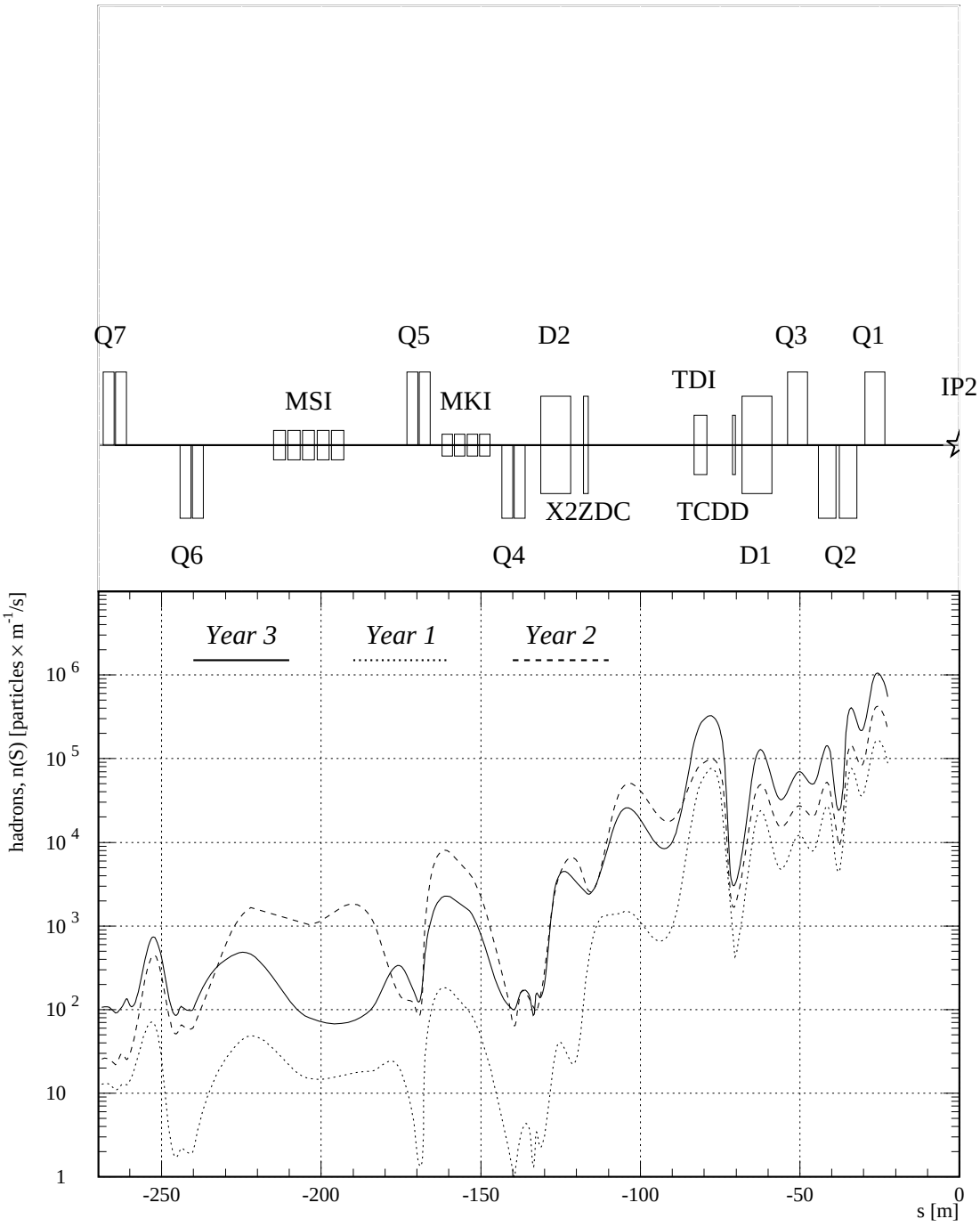

Figure 5: Number of hadrons, entering the UX25 cavern from the IP1 side, as a function of last hadron–nucleus interaction distance to the IP2.

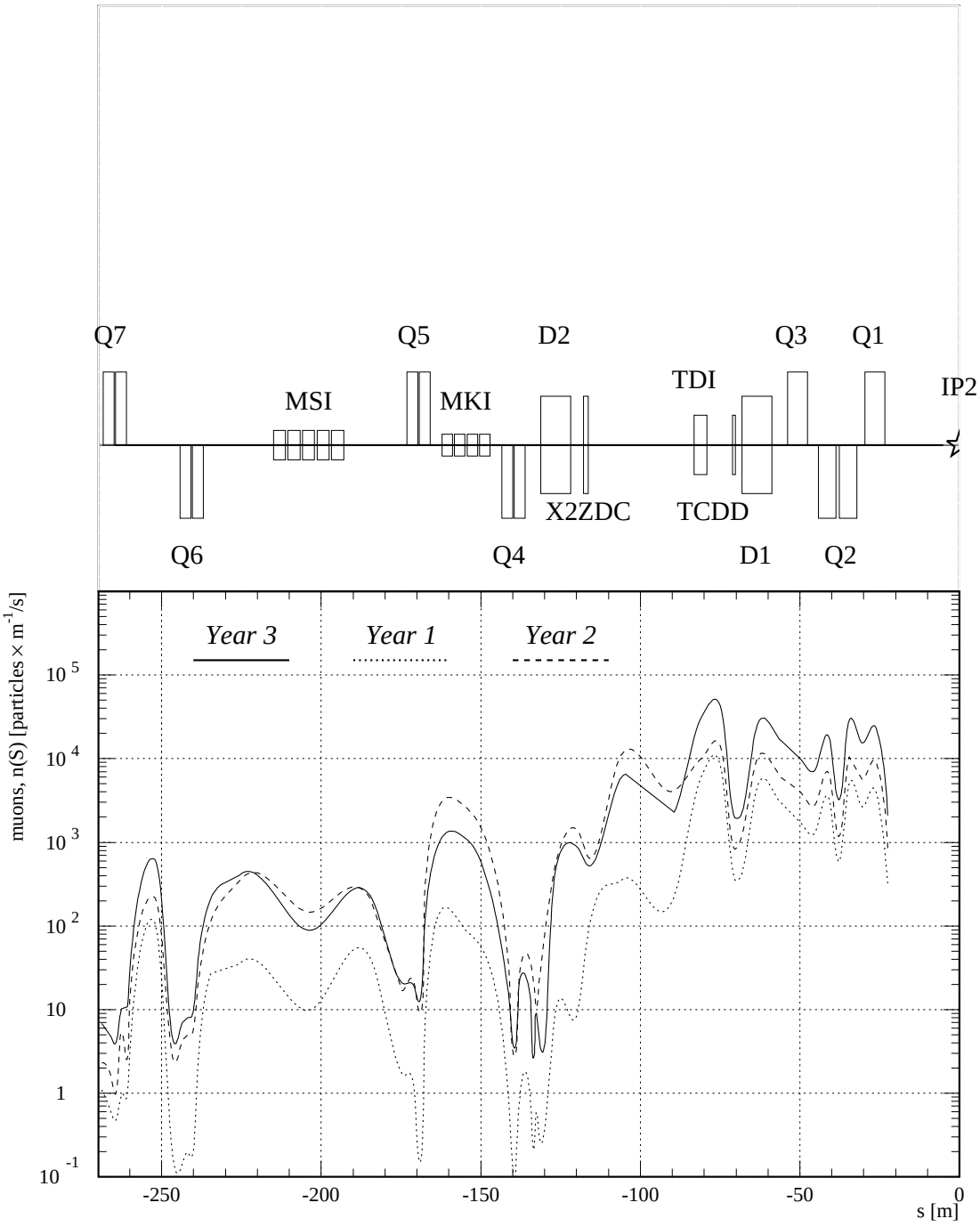

Figure 6: Number of muons, entering the UX25 cavern from the IP1 side, as a function of last hadron–nucleus interaction distance to the IP2.

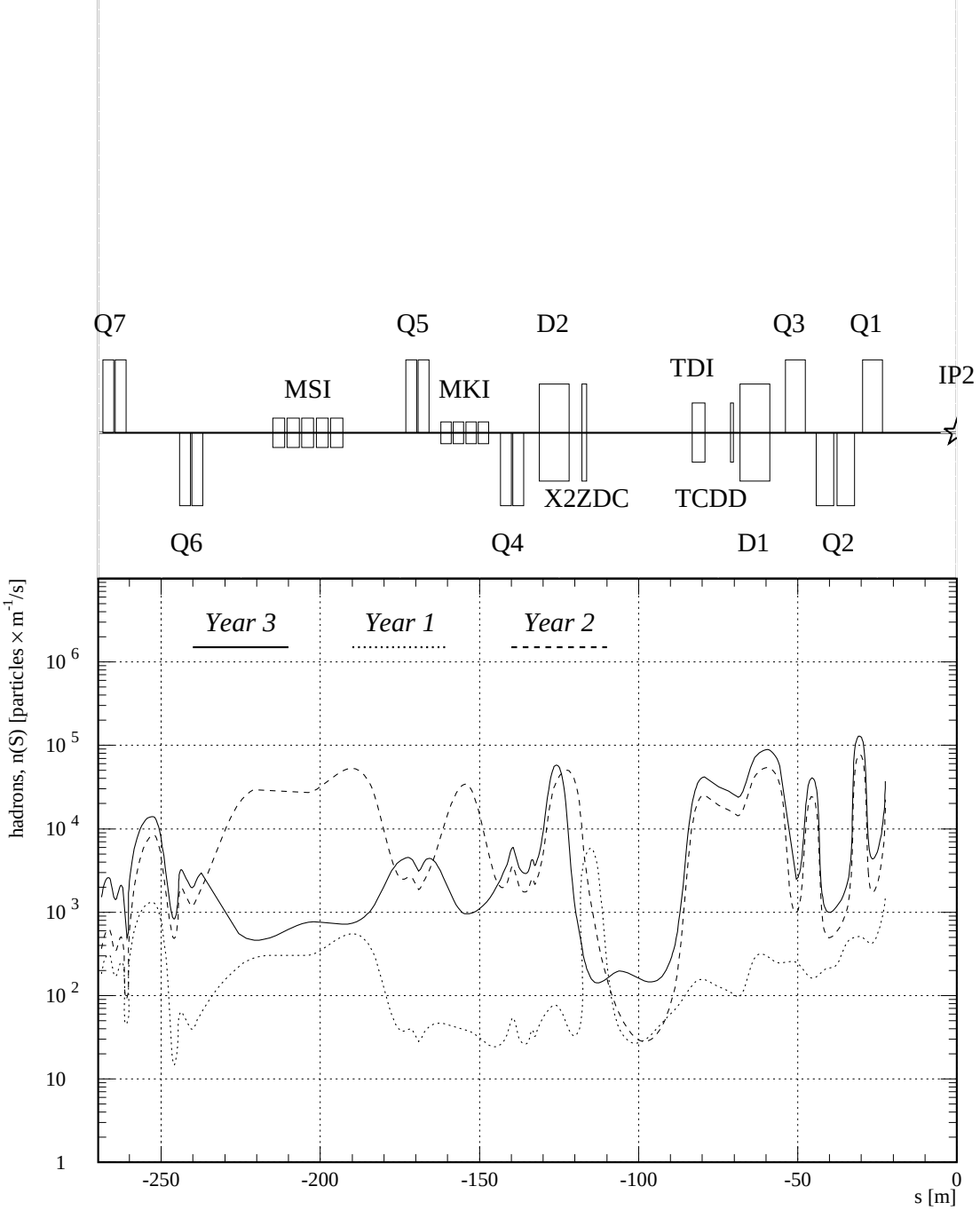

Figure 7: Number of hadrons, entering the UX25 cavern from the IP1 side, as a function of primary proton–nucleus interaction distance to the IP2, assuming the same average gas density in the D1 and TDI.

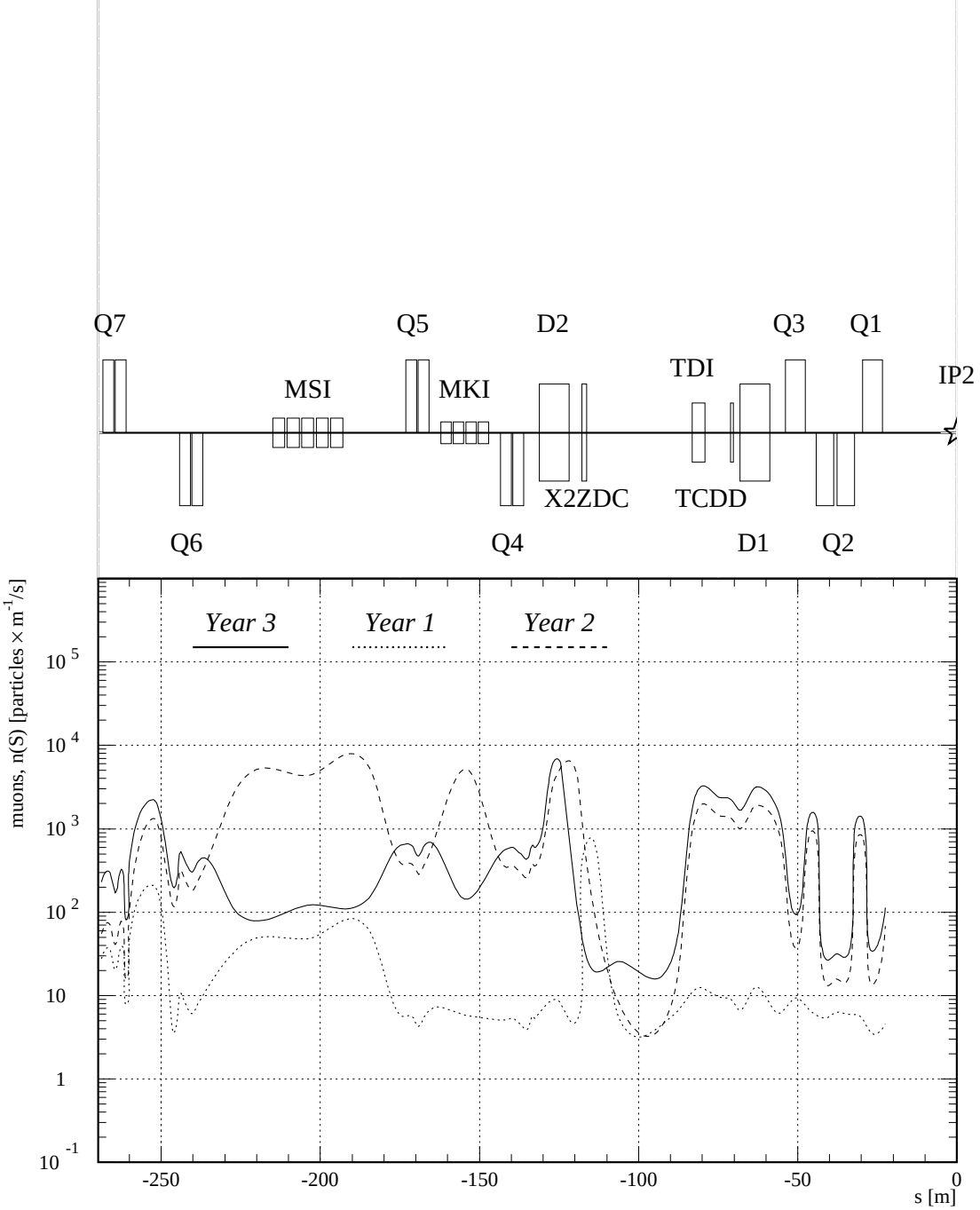

Figure 8: Number of muons, entering the UX25 cavern from the IP1 side, as a function of primary proton–nucleus interaction distance to the IP2, assuming the same average gas density in the D1 and TDI.

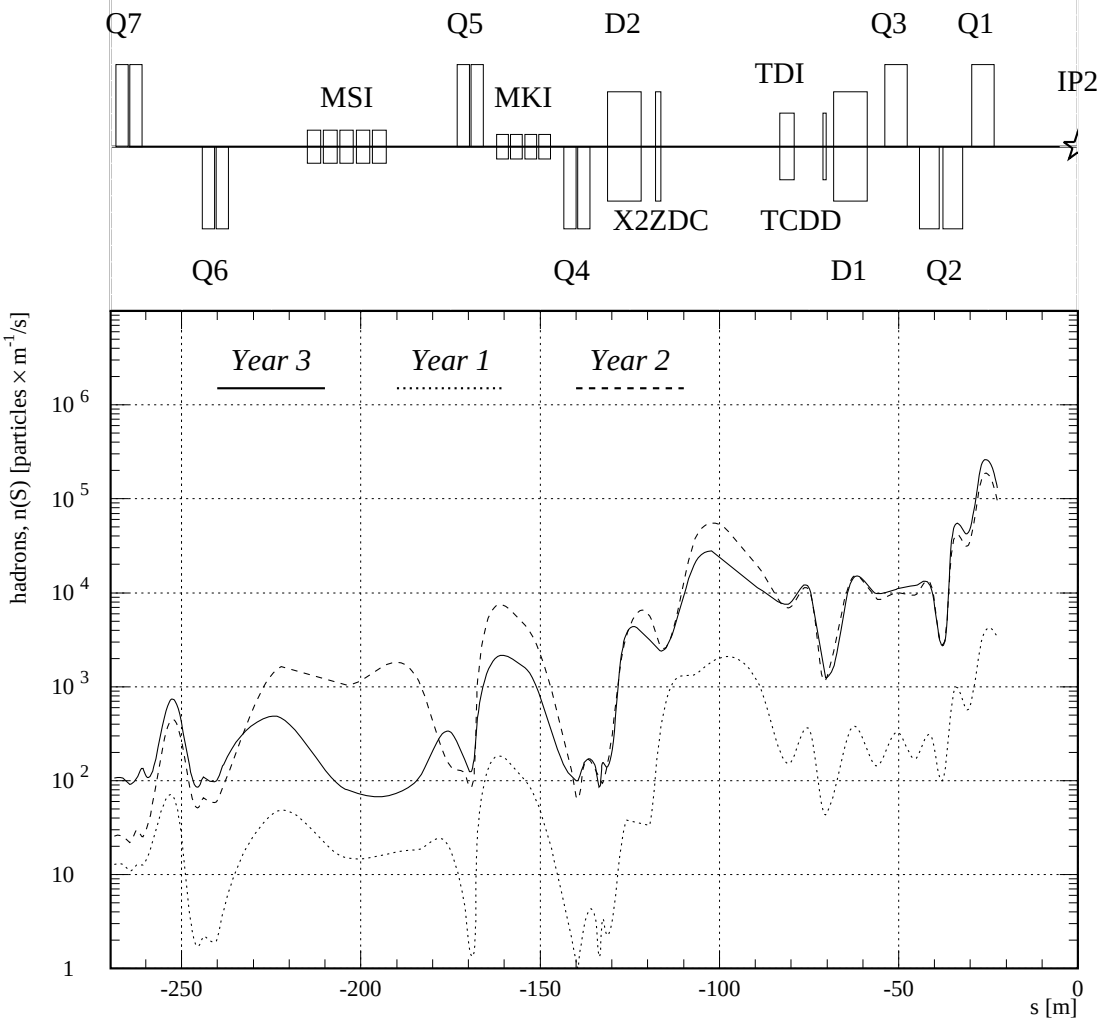

Figure 9: Number of hadrons, entering the UX25 cavern from the IP1 side, as a function of last hadron–nucleus interaction distance to the IP2, assuming the same average gas density in the D1 and TDI.

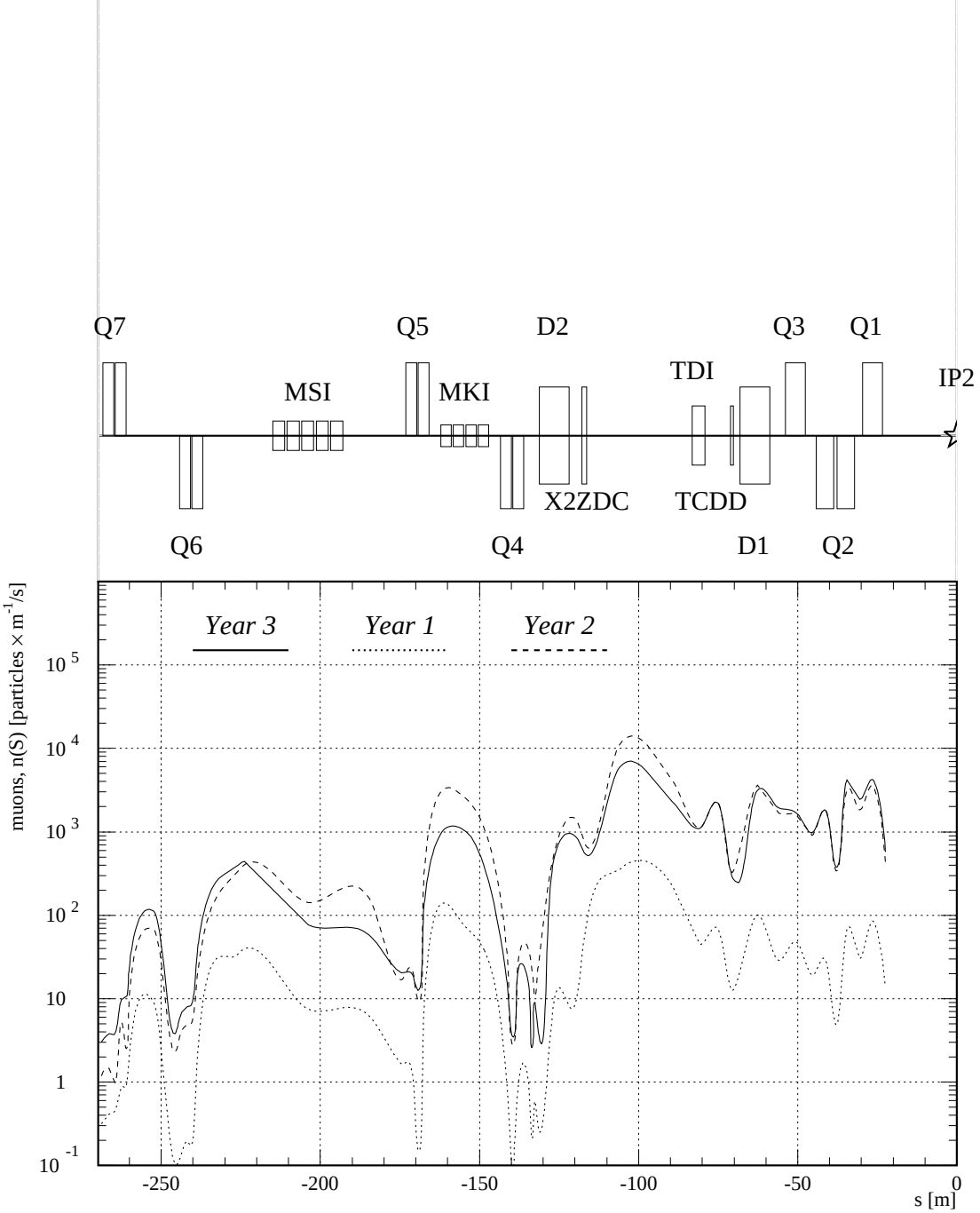

Figure 10: Number of muons, entering the UX25 cavern from the IP1 side, as a function of last hadron–nucleus interaction distance to the IP2, assuming the same average gas density in the D1 and TDI.

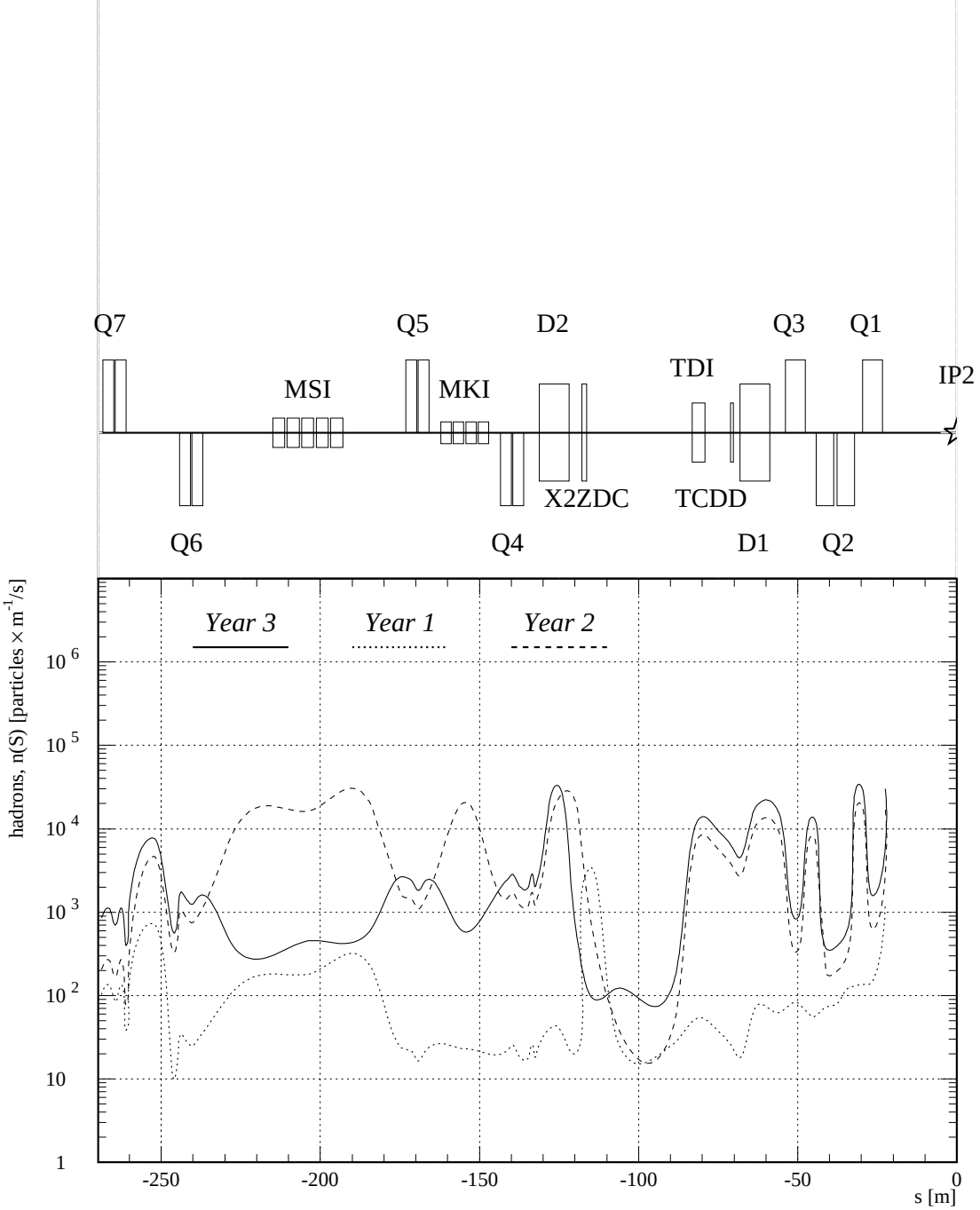

Figure 11: Number of hadrons, entering the UX25 cavern from the IP1 side, as a function of primary proton–nucleus interaction distance to the IP2, assuming the same average gas density in the D1 and TDI, with the 1 GeV cut on the kinetic energy.

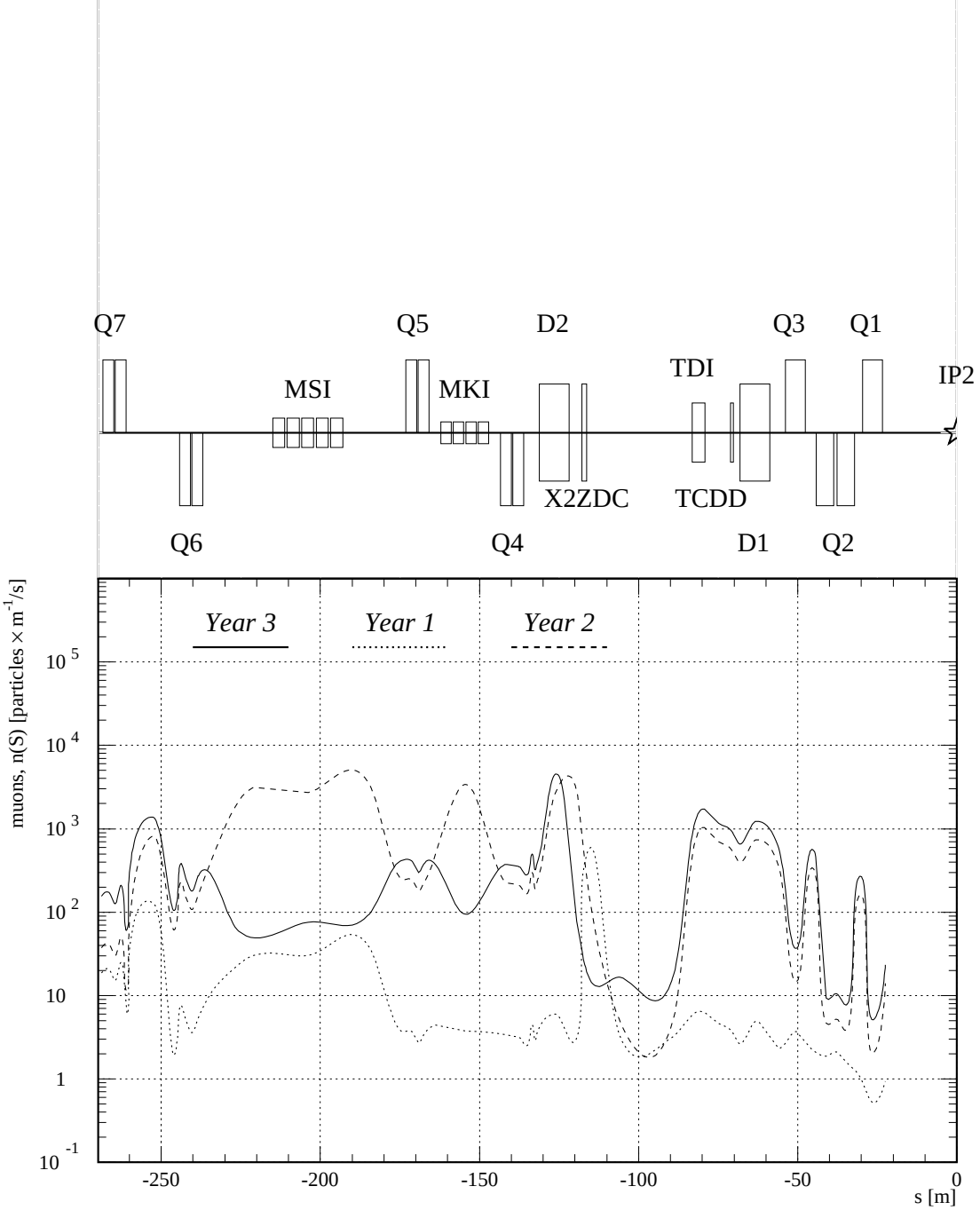

Figure 12: Number of muons, entering the UX25 cavern from the IP1 side, as a function of primary proton–nucleus interaction distance to the IP2, assuming the same average gas density in the D1 and TDI, with the 1 GeV cut on the kinetic energy.

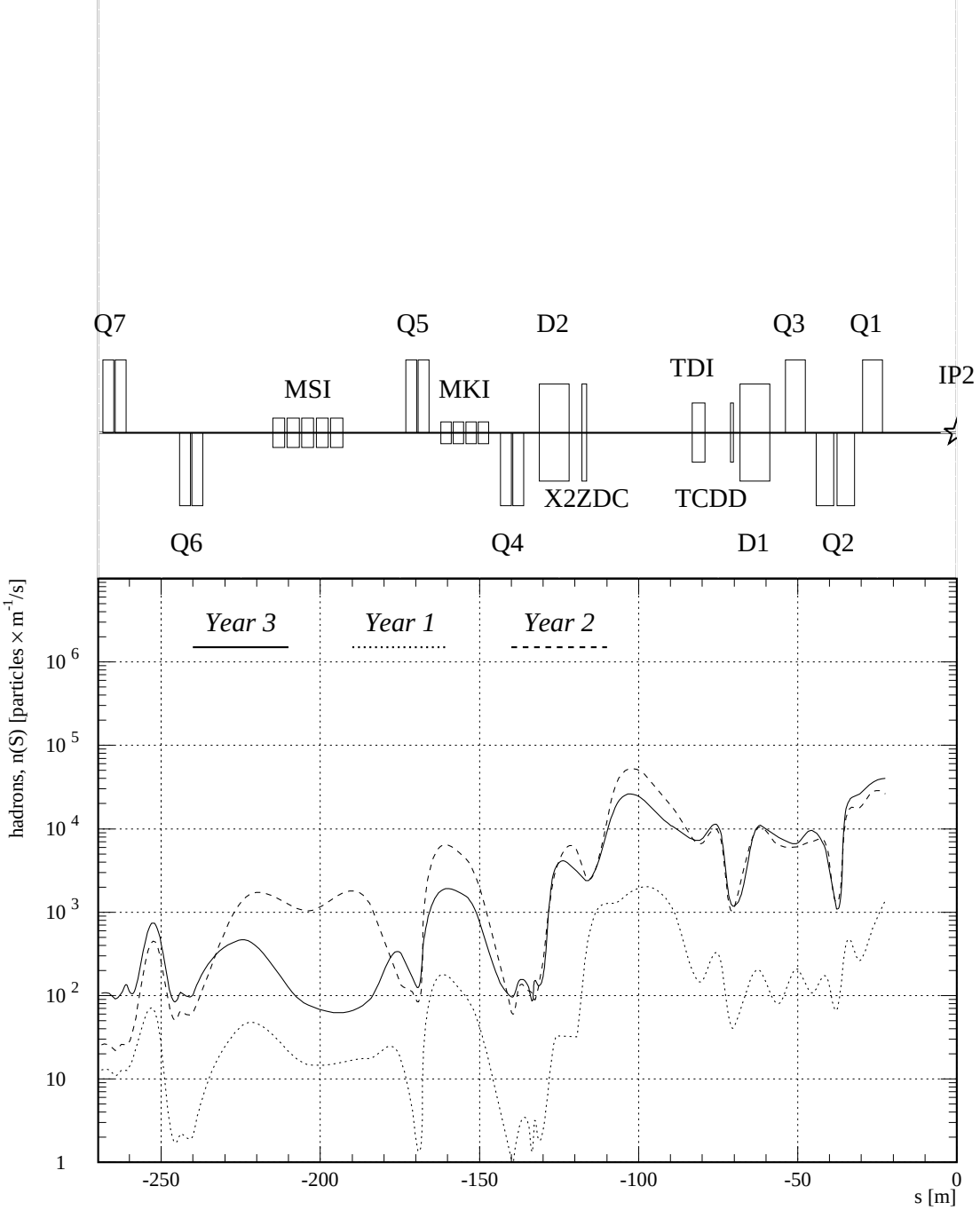

Figure 13: Number of hadrons, entering the UX25 cavern from the IP1 side, as a function of last hadron–nucleus interaction distance to the IP2, assuming the same average gas density in the D1 and TDI, with the 1 GeV cut on the kinetic energy.

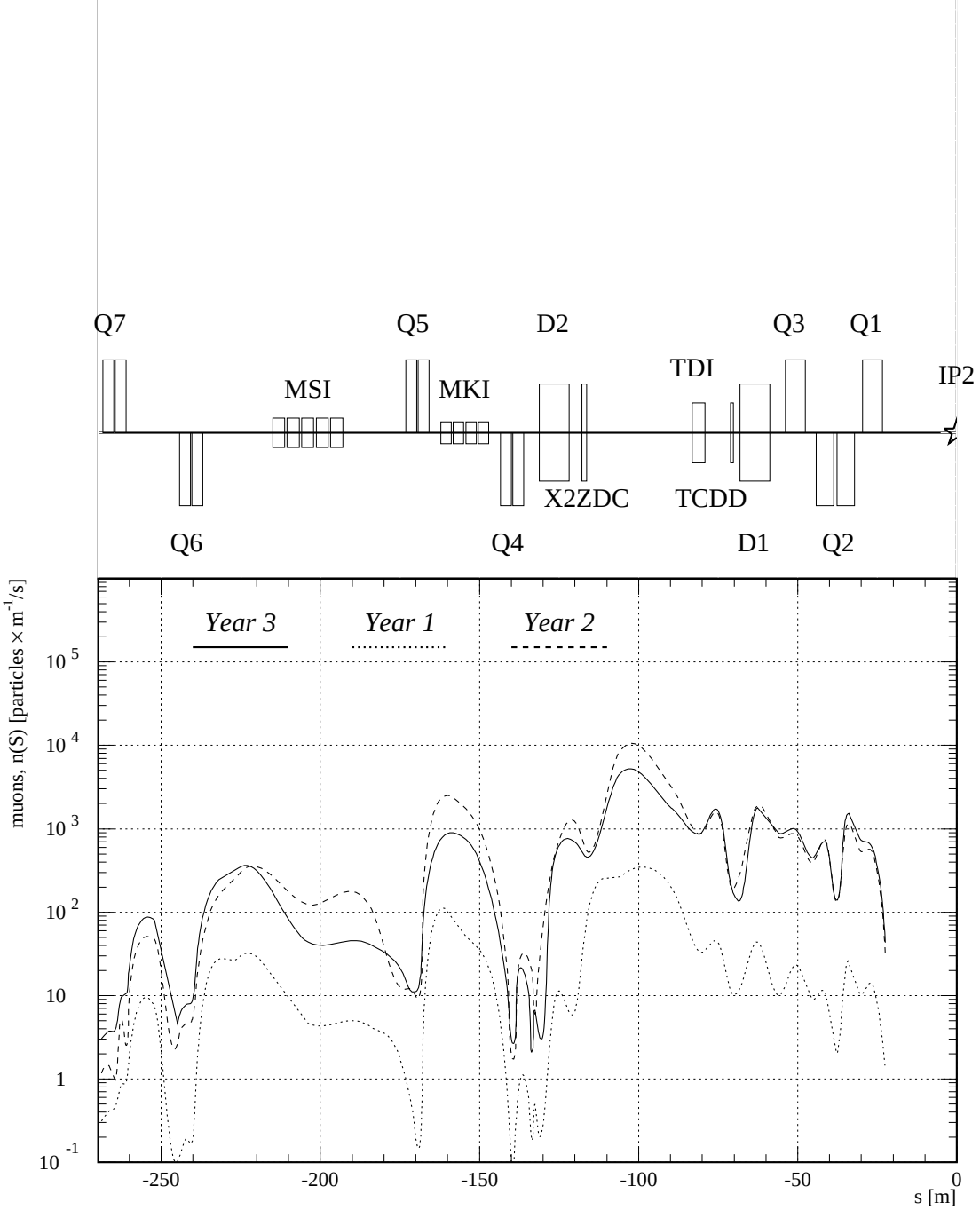

Figure 14: Number of muons, entering the UX25 cavern from the IP1 side, as a function of last hadron–nucleus interaction distance to the IP2, assuming the same average gas density in the D1 and TDI, with the 1 GeV cut on the kinetic energy.

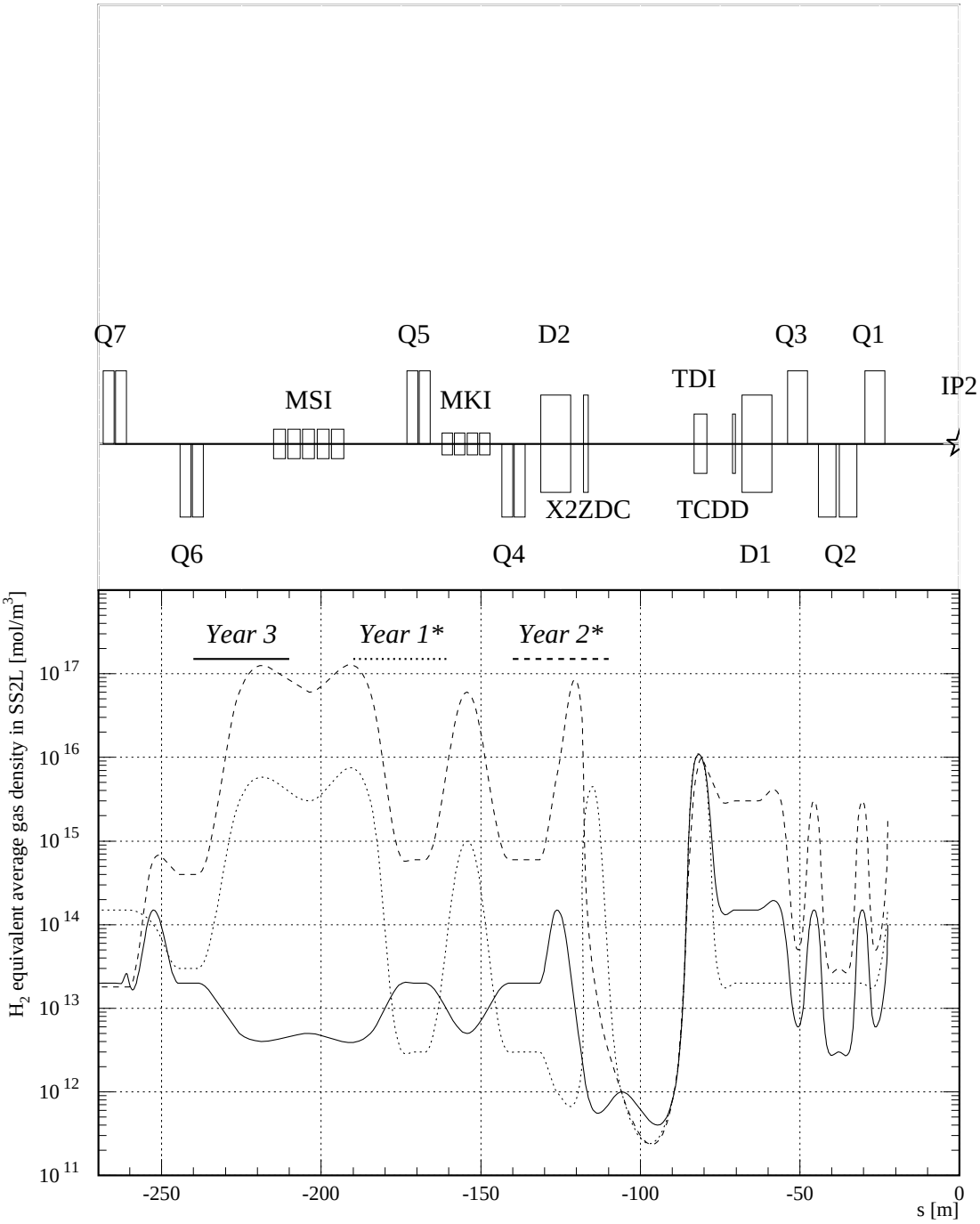

Figure 15: The profiles of H_2 equivalent average gas density in the SS2L, for the beginning of the year 1 and 2.

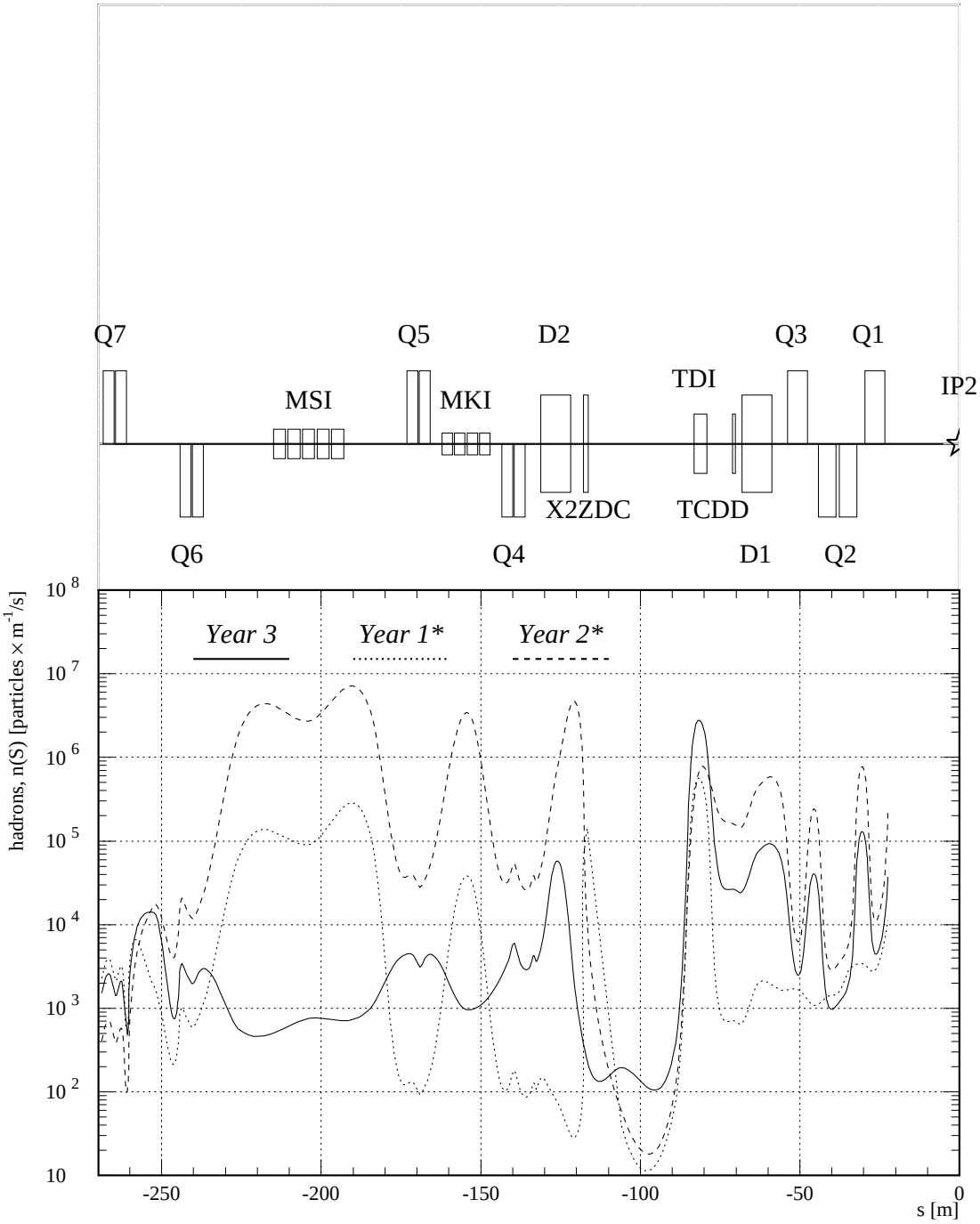

Figure 16: Number of hadrons, entering the UX25 cavern from the IP1 side, as a function of primary proton–nucleus interaction distance to the IP2.

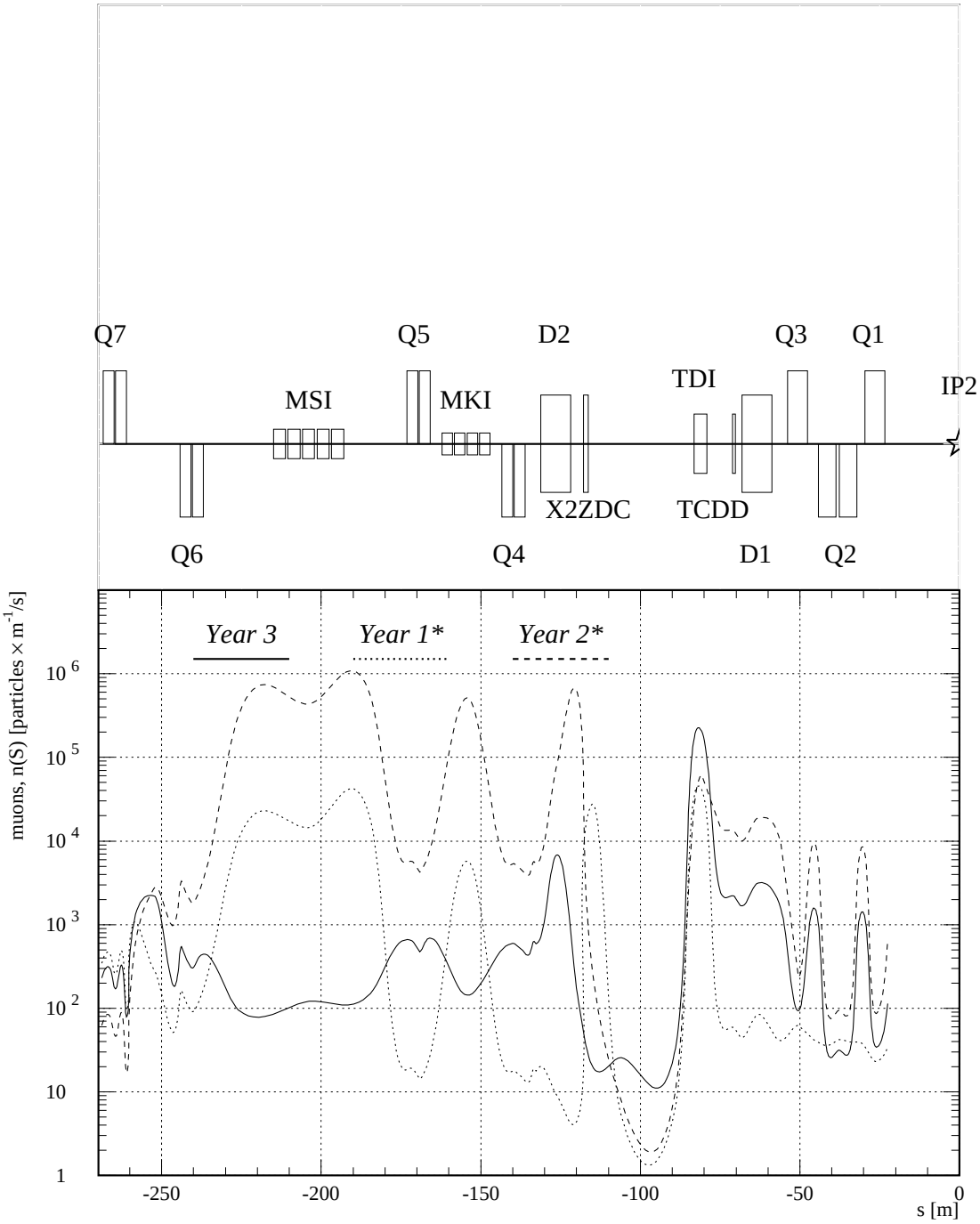

Figure 17: Number of muons, entering the UX25 cavern from the IP1 side, as a function of primary proton–nucleus interaction distance to the IP2.

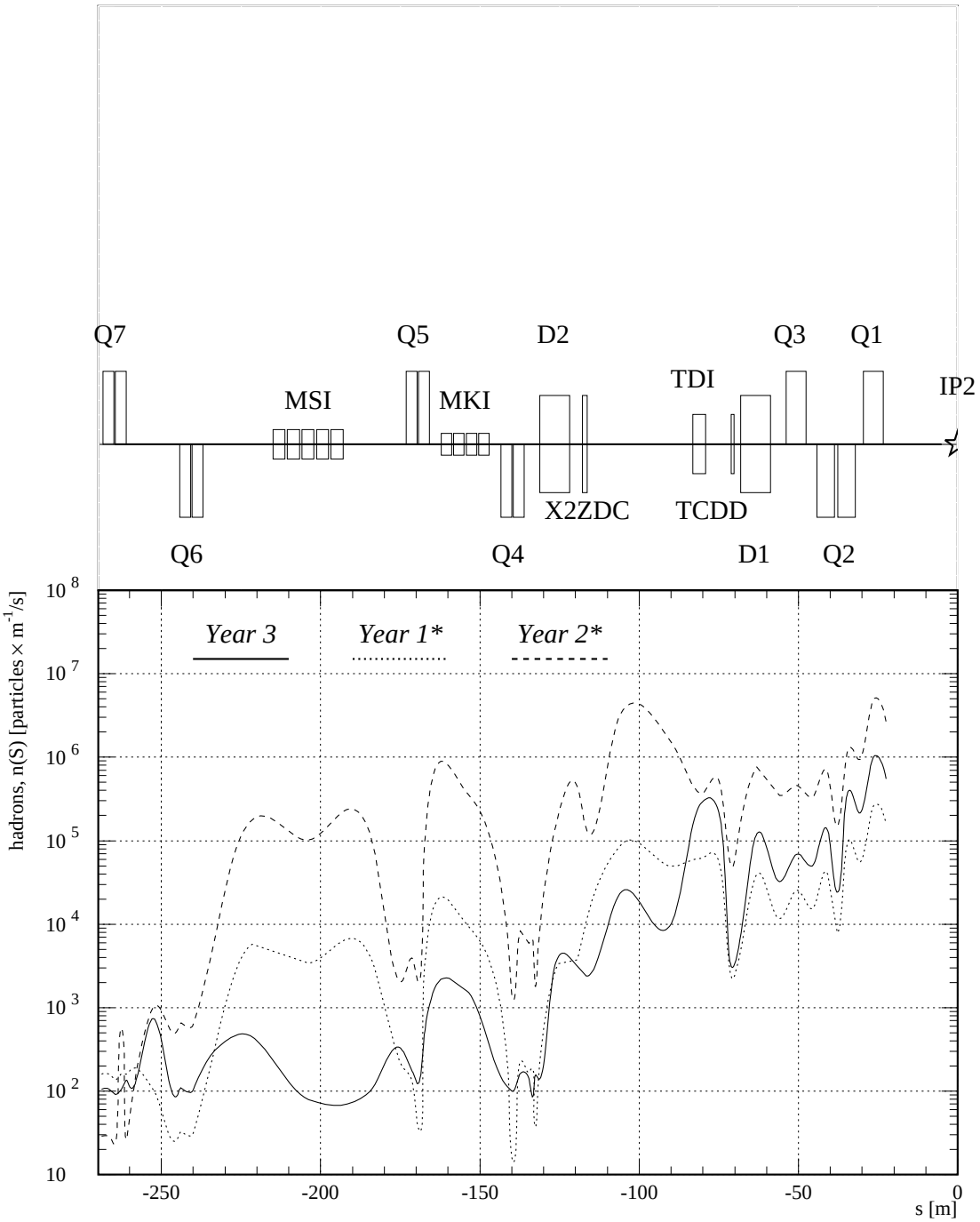

Figure 18: Number of hadrons, entering the UX25 cavern from the IP1 side, as a function of last hadron–nucleus interaction distance to the IP2.

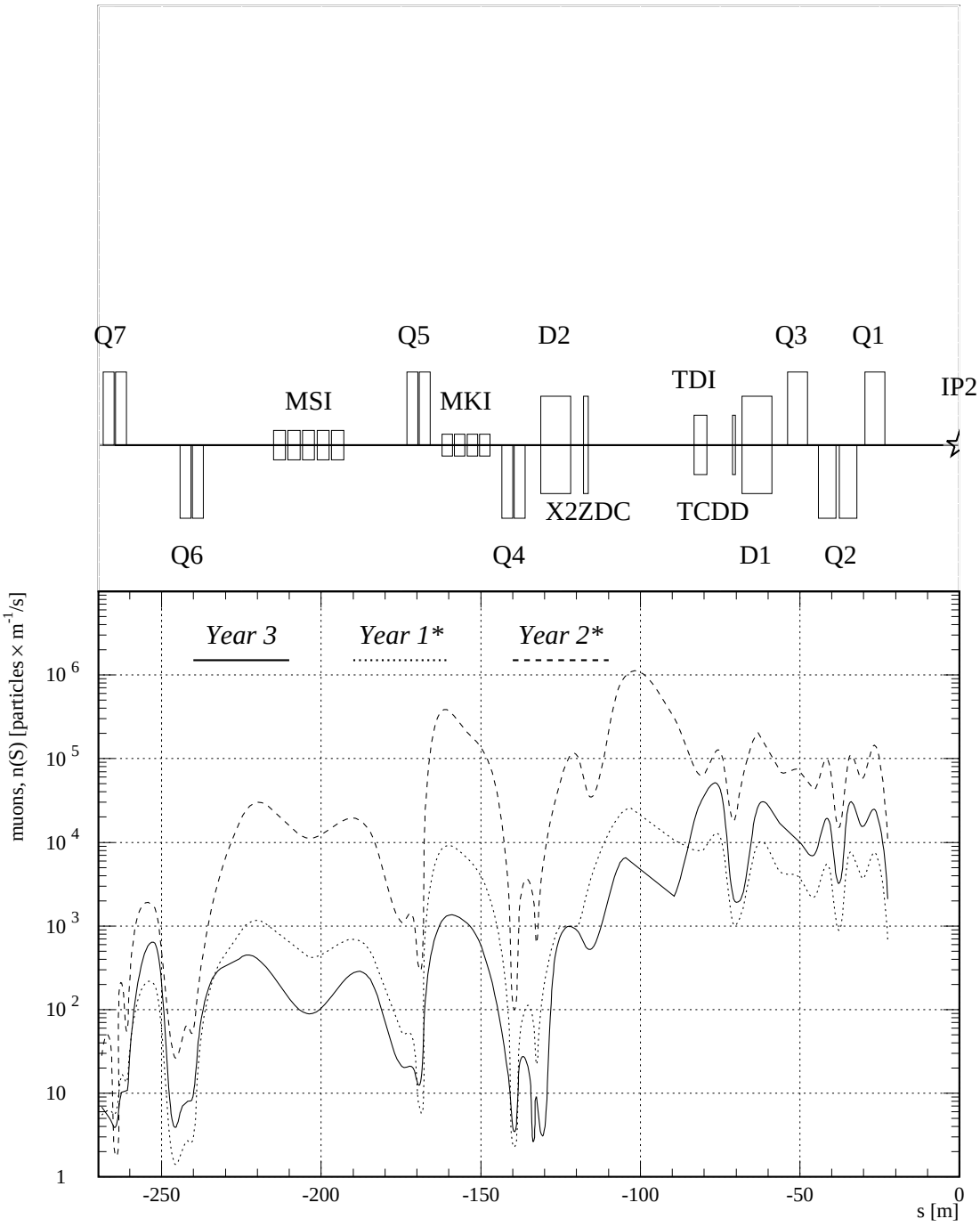

Figure 19: Number of muons, entering the UX25 cavern from the IP1 side, as a function of last hadron–nucleus interaction distance to the IP2.